Available online at www.sciencedirect.com

SCIENCE DIRECT®

Surface & Coatings Technology 196 (2005) 333–340

SURFACE & COATINGS TECHNOLOGY

www.elsevier.com/locate/surfcoat

Microstructural, mechanical, and corrosion characterization of nitrogen-implanted plastic injection mould steel

Orhan Öztürk[a,*], Ortaç Onmuş[a], D.L. Williamson[b]

[a]*Department of Physics, Izmir Institute of Technology, Izmir 35430, Turkey*
[b]*Physics Department, Colorado School of Mines, Golden, CO 80401, USA*

Available online 21 September 2004

Abstract

Nitrogen-ion implantation can be used to improve the wear and corrosion behaviour of moulds for plastic injection by modifying the near-surface layers of these materials. In this study, an FeCr ferritic stainless steel (X36CrMo17, similar to AISI-420F) was ion implanted with 85 keV nitrogen ions to low and high doses of 2×10^{17} and 1×10^{18} ions/cm^2 at a substrate temperature <200 °C in an industrial implantation facility. The N-implanted layer microstructures, thicknesses, and hardnesses were studied by a combination of symmetric and grazing incidence X-ray diffraction (XRD and GIXRD), conversion electron Mössbauer spectroscopy (CEMS), cross-sectional scanning electron microscopy (SEM), and nanohardness measurements. The friction, wear, and corrosion behaviour were investigated by a pin-on-disc tribo tester and a salt spray corrosion analysis method. The XRD, CEMS, and SEM analyses indicate that the N-implanted layers are ~0.05–0.08 μm thick and are composed of ε-$(Fe,Cr,Mn)_{2+x}N$ with paramagnetic and magnetic characteristics. The treated layer shows nearly two times better corrosion resistance than does the substrate. The wear and nanohardness measurements indicate that the wear behaviour and the N-implanted layer hardness are dose dependent and the latter is increased by more than a factor of 1.6 for the high-dose implanted specimen in comparison with that of the substrate material.

Keywords: Nitrogen implantation; Plastic injection mould steels; X-ray diffraction; Mössbauer spectroscopy; Salt spray corrosion; Nanohardness

1. Introduction

The plastics industry is an area of significant technological importance because plastic materials are rapidly replacing many other materials such as wood, paper, metals, and glass. As a consequence, the improvement and performance of production tools in the plastics industry become important. Moulds for plastic injection are normally high cost and quite complicated, consisting of many parts in relative motion with respect to each other and to the plastic, leading to tribological problems in the moulds. Heating during injection moulding causes plastics to liberate gases, resulting in local corrosion and wear of the mould material. In addition, abrasion from the flow of the molten plastic in contact with the tool surfaces, adhesion, release problems on surfaces in contact with the plastics, in which the product sticks to the mould, and fatigue are the most commonly occurring problems [1–3].

Tribological problems associated with the moulding of plastics can often be solved by an appropriate surface modification technique. Ion implantation, compared with various coating techniques (PVD, CVD, and PCVD), and the standard diffusion processes, such as plasma nitriding, can be an efficient surface treatment method, particularly in important niche areas ([1]; industries working with plastics and thin metal/steel sheets). Injection moulds, punches, and dies are often ion implanted with the result that tool life is enhanced by a factor of 3–10 [3]. Injection mould vents are often exposed to corrosive attack from aggressive gases from plastics. Local Cr ion implantation at the vents of the injection moulds can re-alloy the topmost steel surface to a concentration of more than 30 at.% Cr, making it highly corrosion resistant (due to the formation of chromium

* Corresponding author. Tel.: +90 232 750 7513; fax: +90 232 750 7509.
E-mail address: orhanozturk@iyte.edu.tr (O. Öztürk).

0257-8972/$ - see front matter © 2004 Elsevier B.V. All rights reserved.
doi:10.1016/j.surfcoat.2004.08.163

Table 1
Nitrogen ion implantation conditions

Specimen no	Implantation energy (keV)	Dose (ions/cm^2)
S7, S8, S9	85	2×10^{17}
S16, S17, S18	85	1×10^{18}

oxides). In addition to Cr ion implantation, N^+ ion implantation of gates for injection moulding made from cold-working steel results in reduced wear and enhanced tool life [2]. In addition to conventional ion implantation, the plasma immersion ion implantation (PIII) technique is also used in the injection moulding of polymers due to the corrosion and wear deterioration of the mould surface [4]. This treatment method results in a thin nitrided layer, which reduces the adhesion between the polymer and steel and avoids packing during component extraction (during the ejection process, the polymer can get stuck to the mould).

Here, we investigate the influence of conventional nitrogen-ion beam implantation conditions in improving the tribological and corrosion properties of X36CrMo17 injection mould steel (an FeCr ferritic stainless steel). In particular, the hardness, friction, wear, and corrosion behaviour of the N-implanted layers under low and high N ion doses are investigated. Our study combines the use of X-ray diffraction (XRD), conversion electron Mossbauer spectroscopy (CEMS), cross-sectional scanning electron microscopy (SEM), and nanohardness measurements.

2. Experimental

Nitrogen ion implantation into ferritic X36CrMo17 stainless steel, with a base chemical composition Fe-

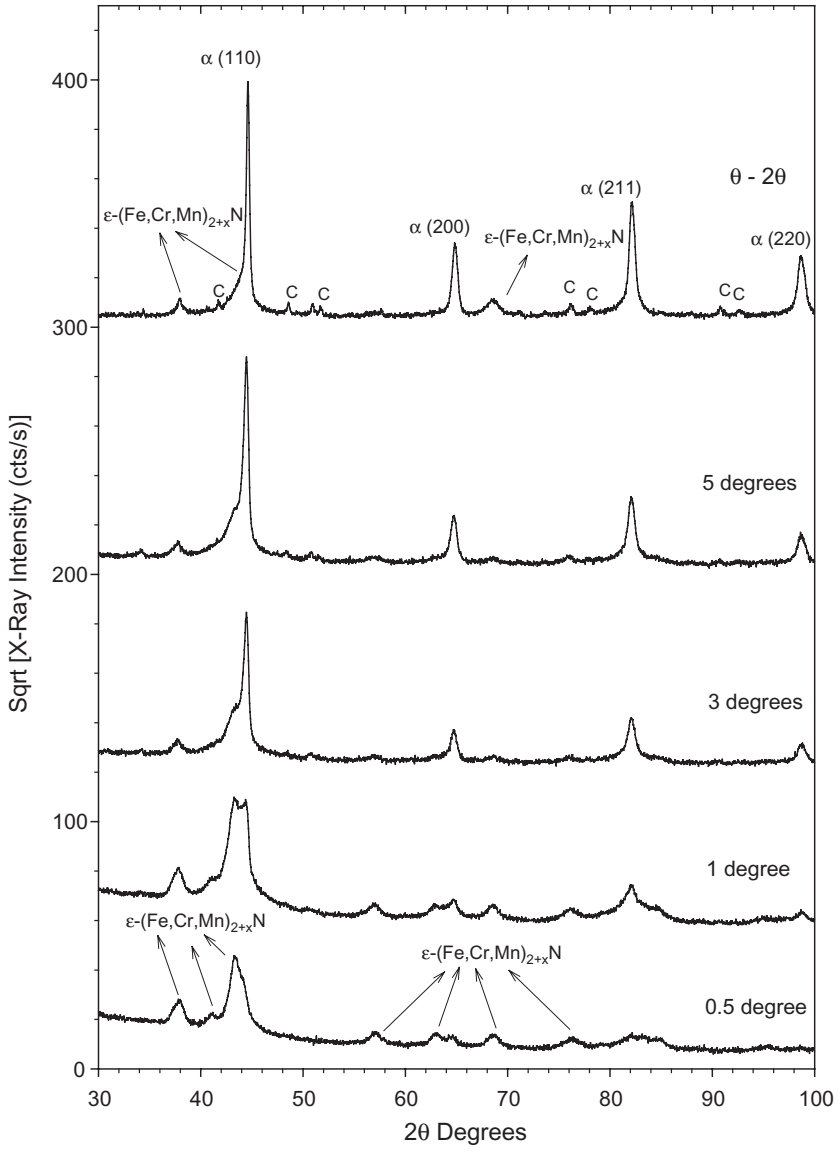

Fig. 1. GIXRD data for the low-dose (2×10^{17} ions/cm^2) nitrogen-implanted specimen. The top data in this figure is the θ–2θ (Bragg–Brentano) scan.

0.33% C-16.7% Cr-1.35% Mn (all in wt.%), was performed in an industrial implantation facility (Implant Sciences). The specimens had a disc-like geometry with a diameter of 3.0 cm and a thickness of 0.30 cm. This geometry was specifically designed for friction and wear analysis before and after the nitrogen implantation. Before implantation, all the specimens were polished to mirror-like quality with a mean surface roughness of about 0.02 μm based on surface profilometry. The polished specimens were implanted with nitrogen ions from the gaseous implanter (ion beam was not mass analyzed) to low and high doses of 2×10^{17} and 1×10^{18} ions/cm^2 at substrate temperatures of <200 °C. The implantation current density was ~1 μA/cm^2. The N-ion implantation conditions for the specimens of this research are summarized in Table 1. Duplicate specimen numbers are listed and used for the various characterization techniques.

XRD was done in both the symmetric θ–2θ Bragg–Brentano and grazing-incidence (GIXRD) modes using a Philips X'pert XRD system in a step-scanning mode (0.05° step size and 4-s count time/step) with Cu-Kα radiation. Conversion electron Mössbauer spectroscopy (CEMS) allowed a quantitative Fe-containing phase analysis of the near-surface region (~0.1 μm [5]). Cross-sectional SEM was done after acid etching in a mixture of HCl and H_2O_2 (1:1 volume ratio) for a few seconds, and nanohardness profiles were obtained using a CSEM tester equipped with a Vickers indentor. Several indentations were made with each of the following loads: 20, 10, 5, 2.5, 1, and 0.5 g. The corrosion behaviour was investigated by a salt spray method (2% NaCl solution in distilled water) and by

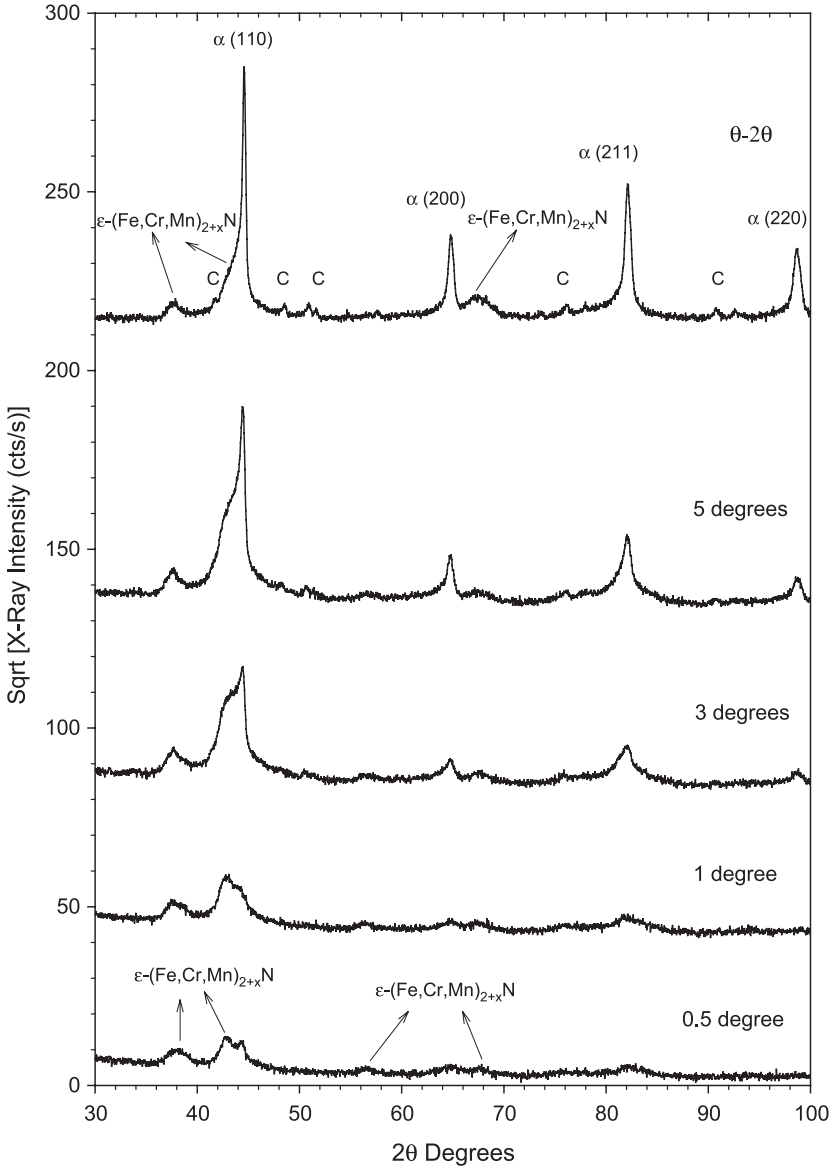

Fig. 2. GIXRD data for the high-dose (1×10^{18} ions/cm^2) nitrogen-implanted specimen. The top data in this figure is the θ–2θ (Bragg–Brentano) scan.

observation (via optical microscopy and SEM) of the acid etching effects of SEM sample preparation. The friction and wear measurements were made by a pin-on-disc wear tester under controlled temperatures and relative humidity of 22–24 °C and ~50%, respectively, and under dry sliding. The contact load was chosen as 1 N (100 g) for the wear tests, yielding a contact stress of about 100 MPa. After the tests, the wear track morphology was investigated with a stylus profilometer.

3. XRD results and discussion

Figs. 1 and 2 show the GIXRD results at the incident angles of 0.1°, 1°, 3°, and 5° for the low-dose, 2×10^{17} ions/cm^2, and high-dose, 1×10^{18} ions/cm^2, nitrogen-implanted specimens. The top data in these figures were obtained by the symmetric θ–2θ scan. The substrate (X36CrMo17) peaks are labeled "α" for the bcc α-(Fe,Cr,Mn) and "C" for the CrFe-carbide phase ($Cr_{-16}Fe_{-7}C_6$), and the implantation-induced ones as ε-$(Fe,Cr,Mn)_{2+x}N$. The GIXRD scans at the incident angles (0.5° and 1°) in Fig. 1 indicate that the top N-implanted layer (~80 nm) is mainly composed of the hexagonal nitride phase ε-$(Fe,Cr,Mn)_{2+x}N$. The effective depths, which is ~sinγ/μ ([6]; where μ is the effective linear mass absorption coefficient) for small incident angles γ, probed by the Cu-Kα X-ray beams at these incident angles are about 38 and 76 nm, respectively. The GIXRD results at higher incident angles (3° and 5°) show more and more contributions coming from the substrate phase [the relative intensities of the substrate α-(Fe,Cr,Mn) peaks compared with the ε-phase peaks increases] due to the increased penetration depths at these angles.

The GIXRD data for the high-dose N-implanted specimen (Fig. 2) also finds the hexagonal nitride phase ε-$(Fe,Cr,Mn)_{2+x}N$ to be distributed in the top implanted layer. The ε peaks of the high-dose implanted specimen are much broader, and their relative intensities are higher compared with the low-dose N-implanted sample. These results demonstrate that the high-dose implanted specimen has a thicker implanted layer with richer N content. However, the sharper nature of the ε-nitride peaks observed for the low-dose N-implanted specimen suggests a more well-defined nitride stoichiometry for this sample compared with the high-dose sample. The broader and asymmetric ε-$(Fe,Cr,Mn)_{2+x}N$ peaks in Fig. 2 suggest a nonuniform nitrogen distribution (i.e., a range of x, variable stoichiometry) or concentration gradient in the implanted layer for the high-dose N-implanted specimen.

4. CEMS results and discussion

Fig. 3 shows the CEMS results for the N-implanted specimens, and Table 2 gives the quantitative Mössbauer

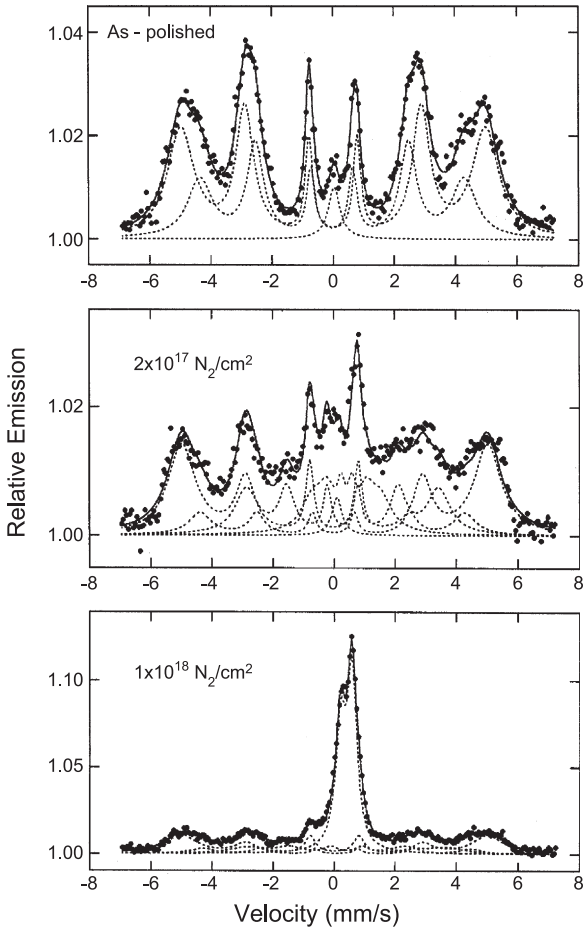

Fig. 3. CEMS data for the substrate material and low- and high-dose nitrogen-ion-implanted specimens.

results for these samples. Also included in the same figure and table are the results for the substrate material. The CEMS spectra of the substrate are composed of magnetic, bcc α-(Fe,Cr,Mn), and paramagnetic components. The magnetic subspectra are consistent with Fe–Cr alloys with a wide range of nearest neighbour environments around the resonant Fe. The small paramagnetic component in Fig. 3 and Table 2 is attributed to Fe in the CrFe-carbide phase, consistent with the XRD results (Figs. 1 and 2). The CEMS spectrum of the low-dose implanted (2×10^{17} ions/cm^2) sample is composed of the magnetic substrate phase [bcc α-(Fe,Cr,Mn)] and additional magnetic resonances whose Mössbauer parameters are quite similar to those of ε-$Fe_{2.67}N$–$Fe_{2.47}N$ reported in the literature [7]. The CEMS results for the high-dose (1×10^{18} ions/cm^2) N-implanted specimen, also shown in Fig. 3, are found to consist of magnetic and paramagnetic components. The magnetic component (H=20.2 T, Table 2) is also attributed to ε-$(Fe,Cr,Mn)_{2+x}N$, with x values similar to those for the low-dose implanted sample and to those in the literature [7]. The strong paramagnetic resonance in the high-dose N-implanted specimen is quite consistent with an Fe_2N-like phase [here, we must have

Table 2
Mössbauer (CEMS) hyperfine parameters and resonance fractions for the low (2×10^{17} ions/cm^2) and high (1×10^{18} ions/cm^2) dose N-implanted specimens

(ions/cm^2)	SS number	CEMS			
		δ	Δ	H	F
As-polished	SS1	+0.01	+0.02	31.0	61
	SS2	−0.04	+0.03	26.9	36
	SS3	+0.04	0	0	3
2×10^{17}	SS1	+00.1 (f)	+0.02 (f)	31.0 (f)	45
	SS2	−0.04 (f)	−0.03 (f)	26.9 (f)	12
	SS3	+0.1	0	0	2
	SS4	+0.035 (f)	0 (f)	19.6	23
	SS5	+0.41 (f)	0 (f)	6.9	18
1×10^{18}	SS1	+0.01 (f)	+0.02 (f)	31.0	30
	SS2	−0.04 (f)	−0.03 (f)	27.2	8
	SS3	+0.40	0.37	0	46
	SS4	+0.26	0 (f)	20.2	16

All measurements were made at room temperature. δ Is the isomer shift (relative to α-Fe) in mm/s, Δ is quadrupole splitting in mm/s, and H is the hyperfine field in Tesla. F is the relative resonance area fraction in percent. The f in parentheses indicates that the parameter was fixed, and SS number refers to the subspectrum number.

ε-(Fe,Cr,Mn)$_{2+x}$N with x~0]; however, the quadrupole splitting parameter (Δ for SS3, Table 2) is somewhat larger than the 0.26–0.29 mm/s values reported for ε-Fe$_2$N in the literature [7].

The quantitative CEMS results in Table 2 demonstrates an average richer N content for the high-dose N-implanted specimen compared with that of the low-dose N-implanted sample. The total resonance fractions of nitrides for the low and high N dose implanted samples are 43% and 62%, respectively, and based on a uniform layer of nitride phase assumption [5], these correspond to the N-implanted layer thicknesses of about 40 and 65 nm, respectively. The N layer thicknesses obtained from the CEMS analysis also correlate reasonably well with TRIM calculations [8]. Based on TRIM, the ballistic depth range for 85 keV N^+ ions is estimated to be ~90 nm (because the non-mass-analyzed beam may contain significant fractions of N_2^+, these ions would lead to ballistics depths of ~45 nm). The CEMS findings of the ε-nitride phase, [ε-(Fe,Cr,Mn)$_{2+x}$N], also correlate quite well with those of the XRD/GIXRD results (Figs. 1 and 2).

5. SEM results and discussion

The cross-sectional SEM data for the low (2×10^{17} ions/cm^2) and high (1×10^{18} ions/cm^2) dose N-implanted specimens (corresponding to SC7 and SC16, Table 1) are given in Fig. 4. Both photomicrographs reveal the N-implanted layer with a relatively uniform thickness. Based on the top and bottom photomicrographs in Fig. 4, the N-implanted layer thicknesses are estimated to be in the range of 0.03 to 0.05 μm and 0.05 to 0.08 μm for the low- and high-dose N-implanted specimens, respectively. The SEM N depths agree quite well with those obtained from the CEMS estimates, which were 40 and 65 nm for the low- and high-dose N implantations.

The photomicrographs in Fig. 4 show that the chemical etch used (HCl+H_2O_2) strongly attacks the substrate phase [α-(Fe,Cr,Mn)], while the ε-(Fe,Cr,Mn)$_{2+x}$N phase is almost unaffected by the same etch. These findings suggest strong etch resistance for the N-implanted layer phase.

6. Corrosion analysis results

In addition to chemical etching during SEM sample preparation, the corrosion behaviour of the nitrogen-implanted specimens was investigated by a salt spray method (ASTM B 117 [9]; 2% NaCl solution in distilled water). The results show that the high-dose N-implanted specimen has a good corrosion resistance. While it takes 3 h for corrosion initiation to occur for the substrate material, the corrosion initiation takes place in 5 h for the high-dose implanted sample. This is attributed to the ε-nitride phase [ε-(Fe,Cr,Mn)$_{2+x}$N], which was found to be distributed in the N-implanted layer based on the GIXRD/XRD and CEMS results. This result also correlates quite well with a literature finding that shows

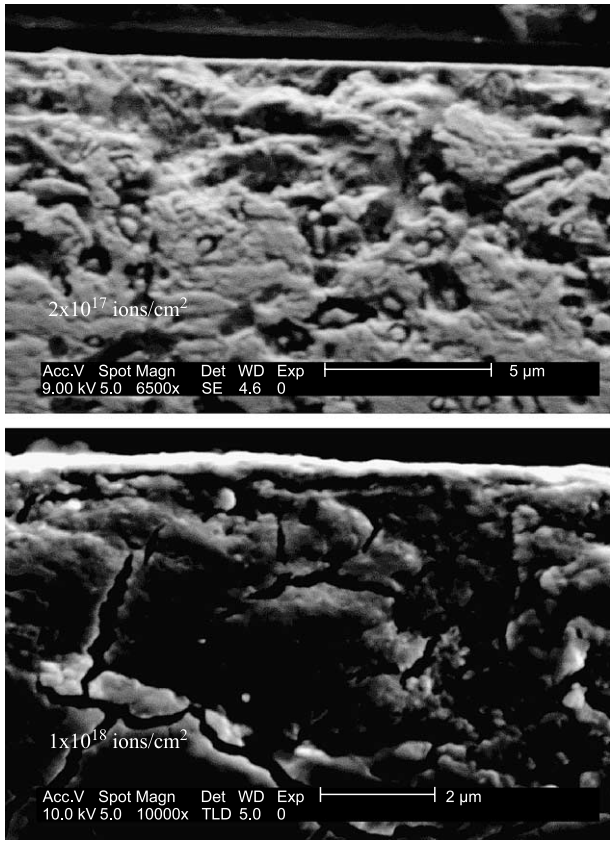

Fig. 4. Cross-sectional SEM photomicrographs for the low- and high-dose N-implanted specimens.

iron nitrides to be more corrosion resistant than ferrite is [10].

7. Nanohardness results and discussion

The average nanohardness values for the nitrogen ion implanted specimens are plotted in Fig. 5 as a function of the indentor load. The hardness values at the lightest load (5 mN) are near ~1150 and ~960 HV for the high- and low-dose N-implanted specimens, respectively, compared with the substrate value, which is about 720 HV, and then continuously decrease to smaller values at larger indentor loads. These results show that the surface hardness values for the N-implanted layer, particularly for the high-dose implanted specimen, increased quite significantly. However, at the lightest load (0.5 g), the indentor penetration depths for the high- and low-dose implanted samples are 0.15 and 0.16 μm, respectively, exceeding the N-implanted layer thicknesses. Therefore, these surface hardness values are not truly representative of the N-implanted layer, and the true hardness values of these layers should be much higher than what is found here. The decrease in hardness at high loads can be explained by the fact that, at high loads, the probe depth of the indentor exceeds the thickness of the implanted layer, resulting in a large contribution of the substrate phase [α-(Fe,Cr,Mn)].

8. Friction and wear results and discussion

Fig. 6 shows the coefficient of friction results obtained during the wear tests, for the N-implanted, as well as for the as-polished, specimens. For the substrate material, a constant high-friction coefficient value was obtained after a short settling period. The average coefficient of friction

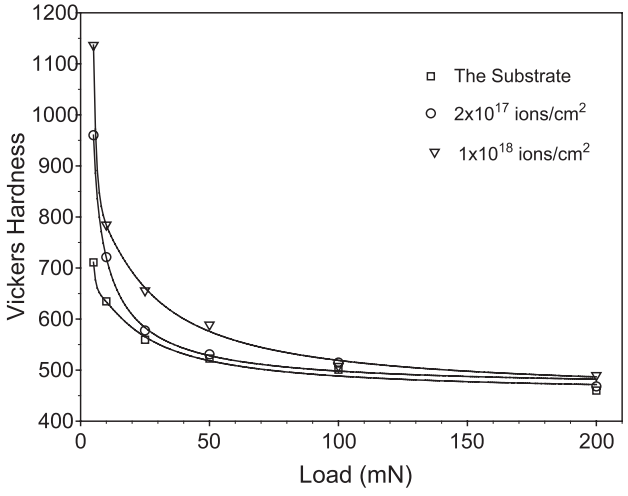

Fig. 5. Nanohardness data for N-implanted samples.

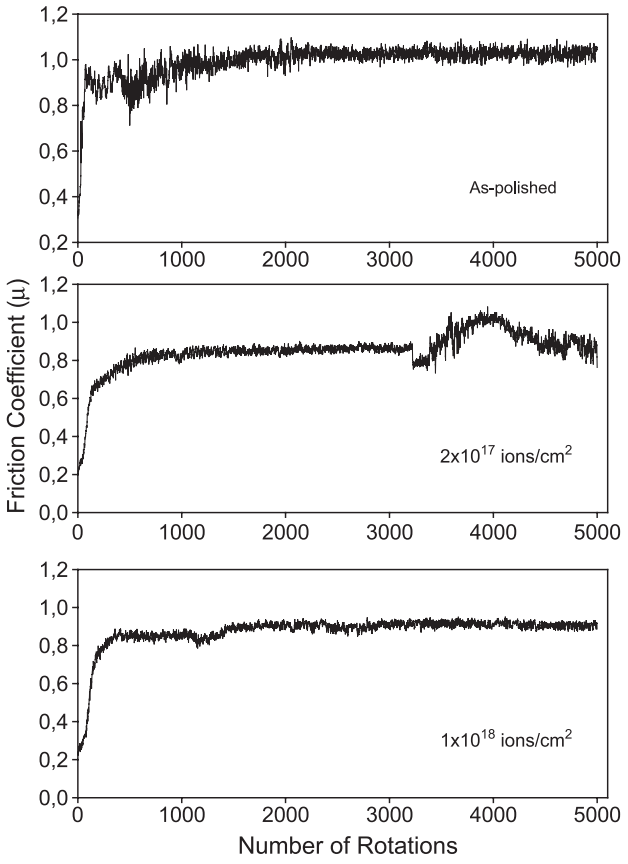

Fig. 6. Friction analysis data for the as-polished and nitrogen-implanted samples.

value for the as-polished sample is found to be 0.99. For the N-implanted specimens, the coefficient of friction values are found to decrease by about 12% for both the low- and high-dose N-implanted specimens. While the friction behaviour for the high-dose N-implanted specimen is quite stable during the course of the experiment (5000 laps), the friction analysis for the low-dose N-implanted specimen (2×10^{17} ions/cm^2) shows an erratic type of behavior over 3200 rotations, implying that the N-implanted layer failed. The average coefficient of friction values found from Fig. 6 for the low- and high-dose N-implanted samples are nearly the same (0.87 and 0.85, respectively), demonstrating that increasing the ion dose does not induce further reduction in the friction coefficient. We believe that the dose mainly increases the load-bearing capacity of the N-implanted layer.

The wear trace morphologies, obtained via surface profilometry, for the as-polished and the low- and high-dose N-implanted specimens are shown in Fig. 7. The average wear trace areas are found to be significantly reduced for the N-ion-implanted specimens. For example, this area for the low-dose N-implanted sample is ~0.2 μm^2, and this represents an 85% drop with respect to the wear trace area of the substrate, which is ~1.3 μm^2. The almost nonexistent depth and width of the wear crater of the high-

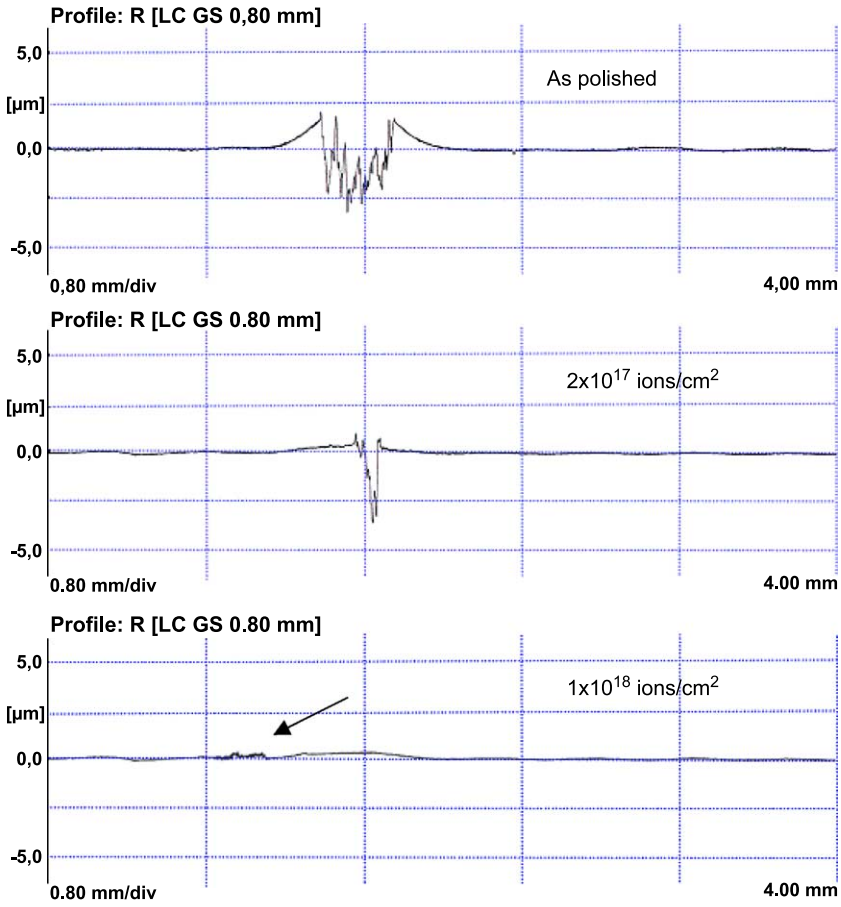

Fig. 7. Wear profiles for N-implanted samples.

dose implanted sample (Fig. 7) compared with the substrate material show that almost no wear is observed over the period of the ball-on-disc wear analysis experiments (5000 laps).

9. Conclusions

The microstructural and tribological properties of low- and high-dose N-implanted specimens of X35CrMo17 injection mould ferritic stainless steel were investigated. Combined XRD and CEMS results show that the plastic injection mould steel implanted with the 85 keV N ions to low (2×10^{17} ions/cm^2) and high (1×10^{18} ions/cm^2) doses leads to a hexagonal type of ε-nitride phase, [ε-$(Fe,Cr,Mn)_{2+x}N$], with both magnetic and paramagnetic characteristics. The nanohardness and salt spray corrosion analysis experiments indicate that both low- and high-dose N-implanted specimens have enhanced wear and corrosion behaviour. In addition, the N-implanted layers are found to have high acid etch resistance based on the SEM sample preparation. The high-dose (1×10^{18} ions/cm^2) specimen has much better wear resistance compared with the low-dose N-implanted sample, and this is attributed to a thicker N-implanted layer (~65 nm based on the CEMS results) with larger N contents. The friction analysis results indicate that the coefficient of friction values are reduced for the N-implanted samples and that increasing the ion dose does not induce further reduction in the friction coefficient value.

Acknowledgments

The study presented here satisfies one of the aims of a larger research and development project (Tubitak-TIDEP No. 3000249) directed by Prof. A. Öztarhan, who is presently affiliated with Tubitak Textile Research Center, Ege University, Izmir, Turkey. The authors would also like to thank Besok Kalipcilik and Donmez Debriyaj for providing the materials for this study and salt spray corrosion tests, respectively.

References

[1] N.J. Mikkelsen, J. Pedersen, C.A. Straede, Surf. Coat. Technol. 158–159 (2002) 42.
[2] Christen A. Straede, Nucl. Instrum. Methods, B 113 (1996) 161.
[3] E.J. Bienk, N.J. Milkelsen, Wear 207 (1997) 6.
[4] S. Rossi, Y. Massiani, E. Bartassi, L. Fedrizzi, Thin Solid Films 416 (2002) 160.

[5] D.L. Williamson, F.M. Kustas, D.F. Fobare, M.S. Misra, J. Appl. Phys. 80 (1986) 1493.
[6] B.D. Cullity, Elements of X-Ray Diffraction, 2nd ed., Addison Wesley, 1978.
[7] G.M. Chen, N.K. Jaggl, J.B. Butt, E.B. Yeh, L.H. Schwartz, J. Phys. Chem. 87 (1983) 5326.
[8] J.F. Ziegler, J.P. Biersack, U. Littmark, TRIM version 92.1.
[9] Website of American Society for Testing and Materials (ASTM), http://www.astm.org.
[10] T. Michler, M. Grischke, K. Bewilogua, H. Dimigen, Thin Solid Films 322 (1998) 206.